M&C 2017 - International Conference on Mathematics & Computational Methods Applied to Nuclear Science & Engineering, Jeju, Korea, April 16-20, 2017, on USB (2017)

Particle Conservation and the Linear Source Method of Characteristics for Isotropic and Anisotropic Sources

Rodolfo M. Ferrer and Joel D. Rhodes III

Studsvik Scandpower, Inc., 1070 Riverwalk Drive, Idaho Falls, Idaho, 83402, rodolfo.ferrer@studsvik.com

Abstract – *Particle conservation is one of the main properties to examine when considering any transport discretization. In the past, particle conservation, i.e., particle balance, has been examined for the 'Flat Source' (FS) approximation used in the Method of Characteristics (MOC) for isotropic and anisotropic sources. The work presented here extends one of the necessary constraints for particle conservation to the recent 'Linear Source' (LS) MOC. As a results, direction-dependent track renormalization and centroids are examined, and a new LS MOC set of equations is derived for problems involving anisotropic scattering. Numerical results are presented which verify that the FS and LS MOC satisfy particle conservation for problems involving isotropic and anisotropic sources by presenting a simple pin cell verification exercise. Finally, results from a set of full-core eigenvalue calculations (updated B&W-1484 Core I & II critical experiments and a hypothetical quarter-core 17x17 PWR model), which make use of the anisotropic source option, are presented and compared in order to evaluate the impact of using either direction dependent or direction independent track renormalization (and centroids.)*

I. INTRODUCTION

The Method of Characteristics (MOC) is a trajectory-based transport discretization that has become the method of choice for solving the neutron transport equation in two-dimensional geometry when performing lattice physics calculations for downstream nodal diffusion reactor analysis and design [1,2]. More recently, the desire to develop explicit, three-dimensional transport methods for full-core calculations has resulted in a renewed interest in the MOC scheme [3-5]. Although conceptually straightforward to generalize to three-dimensions, non-trivial considerations arise when attempting to develop a *practical* MOC scheme for full-core reactor analysis. One example is the use of the Flat Source (FS) approximation, which may require a significant number of source regions in order to obtain a flux solution that is adequately converged in space. The required number of source regions directly impacts the generation and storage of tracking data, which may grow dramatically when considering an explicit full-core calculation. Relaxing the FS approximation in favor of a Linear Source (LS) [6] can reduce the number of source regions necessary to achieve an acceptable level of accuracy.

Recently, the LS approximation for the MOC scheme was implemented into CASMO5 [6] to solve two-dimensional single- and multi-assembly problems in conjunction with the Coarse-Mesh Finite Difference (CMFD) acceleration [7]. Results from numerical tests indicated a significant advantage over the FS approximation for both isotropic [8] and anisotropic sources [9]. In the case of the latter, a reduction in storage was achieved by only considering the zeroth angular moment as spatially linear [6], while treating the high-order angular moments as flat.

The purpose of this work is to fill a perceived gap in the development of the LS MOC scheme as it pertains to particle conservation (also referred to as particle balance) for both isotropic and anisotropic sources. Necessary constraints are introduced in this work for particle conservation in the context of the FS MOC for isotropic and anisotropic sources [10]. These constraints are subsequently generalized for the LS MOC scheme and specific requirements derived involving track renormalization and trajectory-based numerical centroids. Numerical tests are presented which show that the LS MOC does indeed satisfy the particle balance when considering isotropic and anisotropic sources. Practical applications are also presented in order to evaluate the importance of satisfying such constraints, particularly in cases involving anisotropic sources.

II. THEORY

The LS MOC scheme is briefly introduced in this section. A derivation of the LS MOC for anisotropic sources is presented which only considers the zeroth angular moments of the flux as spatially linear. Following the derivation, a constraint is introduced which is used throughout the rest of the work to establish the necessary requirements to satisfy particle balance. This constraint is first applied to the FS MOC under the assumption of isotropic sources. The isotropic-source assumption is relaxed in favor of anisotropic sources and necessary requirements are again obtained from the constraint. An analogous procedure is applied to the LS MOC scheme. The derivation results in requirements that are necessary, but not sufficient, for the LS MOC scheme to satisfy the particle balance.

1. Angular Flux Moments along Tracks

The differential form of the neutron transport equation along a distance s_m in the azimuthal direction a and polar direction p, denoted by $m=(a,p)$, of a track k within source region i is given by

$$\frac{d\psi^g_{m,k,i}}{ds_m} + \Sigma^g_{tr,i}\psi^g_{m,k,i} = q^g_{m,k,i}\left(s_m\right) \qquad (1)$$

where $\psi^g_{m,k,i}$ $q^g_{m,k,i}\left(s_m\right)$, and $\Sigma^g_{tr,i}$ correspond to the angular flux, total source, and transport-corrected total cross section for energy group g, respectively. The linear source along the track length variable s_m is assumed to have the following form

$$q^g_{m,k,i}\left(s_m\right) = \bar{q}^g_{a,k,i} + \hat{q}^g_{m,i}\left(s_m - s^c_{m,k,i}\right). \qquad (2)$$

The entire track length is denoted by $s_{m,k,i}$, such that $0 \le s_m \le s_{m,k,i}$, $s^c_{m,k,i} = s_{m,k,i}/2$, and the expansion coefficients $\bar{q}^g_{a,k,i}$ and $\hat{q}^g_{m,i}$ are defined later on. The integration of Eq. (1) along the track length in cell i yields the characteristics equation

$$\psi^g_{m,k,i}\left(s_m\right) = \psi^g_{m,k,i}\left(0\right) + \left(\frac{\bar{q}^g_{a,k,i}}{\Sigma^g_{tr,i}} - \psi^g_{m,k,i}\left(0\right)\right)F_1\left(\tau^g_m\right) + \frac{\hat{q}^g_{m,i}}{2\left(\Sigma^g_{tr,i}\right)^2}F_2\left(\tau^g_m\right) \qquad (3)$$

where $\tau^g_m = \Sigma^g_{tr,i}s_m$ is a variable optical thickness and $0 \le \tau^g_m \le \tau^g_{m,k,i}$. Functions $F_1\left(\tau^g_m\right)$ and $F_2\left(\tau^g_m\right)$ are defined in [6]. The outgoing angular flux along the track length is obtained by evaluating Eq. (3) at $s_m = s_{m,k,i}$. The balance equation is obtained by integrating Eq. (1) over the track length $s_{m,k,i}$

$$\frac{\psi^g_{m,k,i}\left(s_{m,k,i}\right) - \psi^g_{m,k,i}\left(0\right)}{s_{m,k,i}} + \Sigma^g_{tr,i}\bar{\psi}^g_{m,k,i} = \bar{q}^g_{a,k,i} \qquad (4)$$

where $\bar{\psi}^g_{m,k,i}$ is the track-averaged angular flux. An explicit expression for the first-order spatial moment of the angular flux along each track is obtained by taking the first-order spatial moment of Eq. (3)

$$\hat{\psi}^g_{m,k,i} = \psi^g_{m,k,i}\left(0\right)s^c_{m,k,i} + \left(\frac{\bar{q}^g_{a,k,i}}{\Sigma^g_{tr,i}} - \psi^g_{m,k,i}\left(0\right)\right)\frac{G_1\left(\tau^g_{m,k,i}\right)}{\Sigma^g_{tr,i}} + \frac{\hat{q}^g_{m,i}}{2\left(\Sigma^g_{tr,i}\right)^2}s_{m,k,i}G_2\left(\tau^g_{m,k,i}\right) \qquad (5)$$

where $G_1\left(\tau^g_{m,k,i}\right)$ and $G_2\left(\tau^g_{m,k,i}\right)$ are defined in [6]. Before leaving this section it is worthwhile to note that the proposed scheme conserves the particle balance along each track segment, since no *ad hoc* approximation for the first-order spatial moments is introduced in this derivation. The first-order moment of the angular flux is directly obtained from the exact solution of Eq. (1), which is given by Eq. (3), under the linear source expansion in Eq. (2).

2. Track-based Integration

The numerical integration of f_i and g_i over region i using track data is given by the following expressions

$$\left\langle f,g\right\rangle_{m,i} = \frac{\sin\theta_p}{V_i} \times\sum_k\int_0^{t_{m,k,i}} f_{m,k,i}\left(t'_m\right)g_{m,k,i}\left(t'_m\right)dt'_m\delta A_a \qquad (6)$$

$$\left\langle f,g\right\rangle_i = 4\pi\sum_m \omega_m\left\langle f,g\right\rangle_{m,i} \qquad (7)$$

where δA_a is the width of the characteristic ray, ω_m is the quadrature weight associated with the product quadrature in the m direction, $\sin\theta_p$ is the sine with respect to polar angle θ_p and V_i is the region i volume. Instead of $s_{m,k,i}$, the scaled track length $t_{m,k,i} = \xi_{a,i}s_{m,k,i}$ is used in order highlight the fact that a renormalization procedure is performed, where $\xi_{a,i}$ will be defined shortly. The renormalized track length $t_{m,k,i}$ is used in placed of $s_{m,k,i}$ in the evaluation of Eqs. (3) through (5). Finally, the renormalization is performed by direction and results in the conservation of volume for each region i.

3. Local Coordinate System

A local coordinate system is defined for each mesh cell, centered on $\left(X^c_{a,i}, Y^c_{a,i}\right)$ such that $x = X - X^c_{a,i}$ and $y = Y - Y^c_{a,i}$, where $\left(X,Y\right)$ are the global coordinates. The centroids $\left(X^c_{a,i}, Y^c_{a,i}\right)$ are defined as follows

$$X^c_{a,i} = \left\langle 1, X\right\rangle_{a,i} \qquad (8a)$$

$$Y^c_{a,i} = \left\langle 1, Y\right\rangle_{a,i}. \qquad (8b)$$

The spatial coordinates $\left(X,Y\right)$ are related to t_m via the following equations

$$X\left(t_m\right) = a^x_m t_m/\xi_{a,i} + X^{in}_{a,k,i} \qquad (9a)$$

$$Y\left(t_m\right) = a^y_m t_m/\xi_{a,i} + Y^{in}_{a,k,i} \qquad (9b)$$

where $a_m^x = \cos\varphi_a \sin\theta_p$, $a_m^y = \sin\varphi_a \sin\theta_p$, and $\xi_{a,i}$ is the scaling factor discussed above used to renormalize track lengths in order to conserve volume. Although not unique, the parametrization given by Eqs. (9) results in conservation as long as it is used consistently. Substituting Eqs. (9) into $\langle 1,\cdot\rangle_{m,i}$ and noting that $t_m = t_a / \sin\theta_p$ results in Eqs. (8), in which the angular dependence is reduced to the azimuthal plane. Unlike previous derivations of the LS MOC, the scaling factor $\xi_{a,i}$ is clearly dependent on the angular direction and defined as follows

$$\xi_{a,i} = \frac{V_i}{\delta A_a \sum_k s_{a,k,i}}. \qquad (10)$$

Therefore, the renormalization defined by Eq. (10) results in $\langle 1,1\rangle_{m,i} = 1$, where the $\langle 1,\cdot\rangle_{m,i}$ is defined by Eq. (6).

4. Cell-Averaged Scalar Flux and Isotropic Linear Source

Consider the two-dimensional isotropic linear source approximation

$$q_i^g(x,y) = \frac{1}{4\pi}\left(\bar{q}_i^g + q_{i,x}^g x + q_{i,y}^g y\right). \qquad (11)$$

The coefficients for the source along a track in Eq. (2) are determined by

$$\bar{q}_{a,k,i}^g = \frac{1}{4\pi}\left(\bar{q}_i^g + q_{i,x}^g x_{a,k,i}^c + q_{i,y}^g y_{a,k,i}^c\right) \qquad (12)$$

$$\hat{q}_{m,i}^g = \frac{1}{4\pi}\left(a_m^x q_{i,x}^g + a_m^y q_{i,y}^g\right) / \xi_{i,a} \qquad (13)$$

where $\left(x_{a,k,i}^c, y_{a,k,i}^c\right)$ are the track midpoint coordinates in the local coordinates system. Operating on Eq. (11) with $\langle 1,\cdot\rangle_i$, $\langle x,\cdot\rangle_i$, and $\langle y,\cdot\rangle_i$, results in a 2×2 linear system of equations with coefficients $M_{i,xx}$, $M_{i,yy}$, and $M_{i,xy}$ [6]. The source moments $\vec{Q}_i^g = \left[\bar{q}_i^g, Q_{i,x}^g, Q_{i,y}^g\right]^T$ are obtained by applying

$$\vec{Q}_i^g = \sum_{g'} \Sigma_{s,i}^{g'\to g} \vec{\phi}_i^{g'} + \frac{\chi_i^g}{k} \sum_{g'} \nu\Sigma_{f,i}^{g'} \vec{\phi}_i^{g'} \qquad (14)$$

to the flux moments $\vec{\phi}_i^g = \left[\bar{\phi}_i^g, \Phi_{i,x}^g, \Phi_{i,y}^g\right]^T$, where $\Sigma_{s,i}^{g'\to g}$ is the scattering cross section matrix, $\nu\Sigma_{f,i}^g$ is the nu-fission cross section, χ_i^g is the fission spectrum, and k is the eigenvalue. The spatial moments of the scalar flux are obtained by substituting $\psi_{m,k,i}^g(t_m)$ into $\langle 1,\cdot\rangle_i$, $\langle x,\cdot\rangle_i$, and $\langle y,\cdot\rangle_i$, which results in the following set of equations

$$\bar{\phi}_i^g = \frac{\bar{q}_i^g}{\Sigma_{tr,i}^g} + \frac{4\pi}{\Sigma_{tr,i}^g V_i} \sum_a \bar{\omega}_a \sum_p \bar{\omega}_p \sum_k \Delta_{m,k,i}^g \qquad (15)$$

$$\Phi_{i,x}^g = \frac{q_{i,x}^g}{\Sigma_{tr,i}^g} C_{i,x}^g + \frac{q_{i,y}^g}{\Sigma_{tr,i}^g} C_{i,xy}^g + \frac{4\pi}{\Sigma_{tr,i}^g V_i} \sum_a \bar{\omega}_a \sum_p \bar{\omega}_p \times \sum_k \left[\cos\varphi_a s_{a,k,i} \psi_{m,k,i}^g(0) H\left(\tau_{m,k,i}^g\right) + x_{a,k,i}^{in} \Delta_{m,k,i}^g\right] \qquad (16)$$

$$\Phi_{i,y}^g = \frac{q_{i,y}^g}{\Sigma_{tr,i}^g} C_{i,y}^g + \frac{q_{i,x}^g}{\Sigma_{tr,i}^g} C_{i,xy}^g + \frac{4\pi}{\Sigma_{tr,i}^g V_i} \sum_a \bar{\omega}_a \sum_p \bar{\omega}_p \times \sum_k \left[\sin\varphi_a s_{a,k,i} \psi_{m,k,i}^g(0) H\left(\tau_{m,k,i}^g\right) + y_{a,k,i}^{in} \Delta_{m,k,i}^g\right] \qquad (17)$$

where $\bar{\omega}_p = \omega_p \sin\theta_p$, $\bar{\omega}_a = \omega_a \delta A_a$, $\Delta_{m,k,i}^g = \left[\psi_{m,k,i}^g(0) - \psi_{m,k,i}^g\left(t_{m,k,i}\right)\right]$, and $H\left(\tau_{m,k,i}^g\right)$, $C_{i,x}^g$, $C_{i,y}^g$, and $C_{i,xy}^g$ are defined in [6].

5. Cell-Averaged Scalar Flux and Anisotropic Linear Source

Consider the anisotropic source in region i, which is analogous to the isotopic case defined by Eq. (11),

$$q_{m,i}^g(x,y) = \frac{1}{4\pi}\left(\bar{q}_{m,i}^g + q_{i,x}^g x + q_{i,y}^g y\right). \qquad (18)$$

The coefficients of the track source $\bar{q}_{m,k,i}^g$ and $\hat{q}_{m,i}^g$ are analogous to those given by Eqs. (12) and (13), except for the fact that $\bar{q}_i^g \to \bar{q}_{m,i}^g$. Operating on Eq. (18) with $\langle 1,\cdot\rangle_i$, $\langle x,\cdot\rangle_i$, and $\langle y,\cdot\rangle_i$, results in a 2×2 linear system of equations with coefficients $M_{i,xx}$, $M_{i,yy}$, and $M_{i,xy}$ [6]. The linear expansion coefficients in Eq. (18) presuppose analogous expansion coefficients for the flux, e.g., $\phi_{i,x}^g$ and $\phi_{i,y}^g$. Therefore, the source moments $\left\{Q_{i,x}^g, Q_{i,y}^g\right\}$ can be obtained by applying Eq. (14) to $\left\{\Phi_{i,x}^g, \Phi_{i,y}^g\right\}$, which follow the development of the linear source in the isotropic case. However, the evaluation of the constant (or average) angular source requires the use of the moment-to-discrete operator

$$\bar{q}_{m,i}^{g} = \sum_{l=0}^{L}\sum_{r=-l}^{l} R_{\alpha}\left(\varphi_a,\mu_p\right)\sum_{g'}\Sigma_{s,i}^{g'\to g,l}\bar{\phi}_i^{g',\alpha} + \frac{\chi_i^g}{k}\left(\sum_{g'}\nu\Sigma_{f,i}^{g'}\bar{\phi}_i^{g'}\right) \tag{19}$$

where L is the anisotropic scattering expansion order, $\mu_p = \cos\theta_p$, $\alpha = (l,r)$ is a double index, and $R_{\alpha}\left(\varphi_a,\mu_p\right)$ is the real spherical harmonics function. Higher-order scattering matrices $\Sigma_{s,i}^{g'\to g,l}$ are necessary in order to evaluate Eq. (19) for $L > 0$. In the so-called LS+P0 approach [6] the angular moments of the angular flux are accumulated during the transport sweep by substituting $\psi_{m,k,i}^{g}(t_m)$ into $\left\langle 1, R_{\alpha}\left(\varphi_a,\mu_p\right)\cdot\right\rangle_i$, $\left\langle x,\cdot\right\rangle_i$, and $\left\langle y,\cdot\right\rangle_i$, which results in the following set of equations

$$\bar{\phi}_i^{g,\alpha} = \sum_a \omega_a \sum_p \omega_p R_{\alpha}\left(\varphi_a,\mu_p\right)\frac{\bar{q}_{m,i}^{g}}{\Sigma_{T,i}^{g}} + \frac{4\pi}{\Sigma_{T,i}^{g}V_i}\sum_a\bar{\omega}_a\sum_p\bar{\omega}_p R_{\alpha}\left(\varphi_a,\mu_p\right)\sum_k\Delta_{m,k,i}^{g} \tag{20}$$

$$\Phi_{i,x}^{g} = \frac{q_{i,x}^{g}}{\Sigma_{T,i}^{g}}C_{i,x}^{g} + \frac{q_{i,y}^{g}}{\Sigma_{T,i}^{g}}C_{i,xy}^{g} + \frac{4\pi}{\Sigma_{T,i}^{g}V_i}\sum_a\bar{\omega}_a\sum_p\bar{\omega}_p \times\sum_k\left[\cos\varphi_a s_{a,k,i}\psi_{m,k,i}^{g}(0)H\left(\tau_{m,k,i}^{g}\right) + x_{a,k,i}^{in}\Delta_{m,k,i}^{g}\right] - \frac{4\pi}{\Sigma_{T,i}^{g}V_i}\sum_a\bar{\omega}_a\sum_p\bar{\omega}_p\frac{\bar{q}_{m,i}^{g}}{4\pi\Sigma_{T,i}^{g}}\sum_k\cos\varphi_a s_{a,k,i}H\left(\tau_{m,k,i}^{g}\right) \tag{21}$$

$$\Phi_{i,y}^{g} = \frac{q_{i,y}^{g}}{\Sigma_{T,i}^{g}}C_{i,y}^{g} + \frac{q_{i,x}^{g}}{\Sigma_{T,i}^{g}}C_{i,xy}^{g} + \frac{4\pi}{\Sigma_{T,i}^{g}V_i}\sum_a\bar{\omega}_a\sum_p\bar{\omega}_p \times\sum_k\left[\sin\varphi_a s_{a,k,i}\psi_{m,k,i}^{g}(0)H\left(\tau_{m,k,i}^{g}\right) + y_{a,k,i}^{in}\Delta_{m,k,i}^{g}\right] - \frac{4\pi}{\Sigma_{T,i}^{g}V_i}\sum_a\bar{\omega}_a\sum_p\bar{\omega}_p\frac{\bar{q}_{m,i}^{g}}{4\pi\Sigma_{T,i}^{g}}\sum_k\sin\varphi_a s_{a,k,i}H\left(\tau_{m,k,i}^{g}\right) \tag{22}$$

where the angular dependence of the centroids results in the $\delta A_a\sum_k x_{a,k,i}^{c}t_{a,k,i} = 0$ and $\delta A_a\sum_k y_{a,k,i}^{c}t_{a,k,i} = 0$. Eqs. (20) through (22) reduce to Eqs. (15) through (17) by only considering the isotropic case $\bar{q}_{m,i}^{g}\to\bar{q}_i^{g}$ and the zeroth angular moments of the angular flux. Eqs. (43)-(45) from [6] become (20)-(22) if Eqs. (18) and (10) are applied.

6. Particle Conservation and the Flat Source MOC

Particle conservation and anisotropy for trajectory-based methods has been previously examined by other authors [10]. In that particular work, the authors examine quadrature-related constraints that are necessary to ensure particle conservation. In addition, a constraint is introduced using the trajectory-based spatial moments such that the trajectory sources integrate exactly to the angular moments of the source over a region. In the case of the FS, the constraint can be re-stated as follows

$$\left\langle 1, R_{\alpha}\left(\varphi_a,\mu_p\right)\frac{1}{4\pi}\bar{q}_{m,i}^{g}\right\rangle_i = \bar{q}_i^{g,\alpha} \tag{23}$$

where $\bar{q}_i^{g,\alpha}$ is the angular moment of the anisotropic source in region i. In the case of an isotropic source, only the zeroth-order angular moment is of interest and Eq. (23) reduces to the following expression

$$\left\langle 1, \frac{1}{4\pi}\bar{q}_i^{g}\right\rangle_i = \bar{q}_i^{g}. \tag{24}$$

As noted in [10], Eq. (24) is satisfied by either direction-dependent or independent renormalization of the tracks. In the latter case, Eq. (10) becomes

$$\xi_i = \frac{V_i}{\sum_a\omega_a\delta A_a\sum_k s_{a,k,i}}. \tag{25}$$

The renormalization given by Eq. (25) is applied in the majority of FS MOC implementations when considering an isotropic source. However, in the case of anisotropic sources, Eq. (23) can be further developed by first expanding the directional source using the spherical harmonics as a basis

$$\bar{q}_{m,i}^{g} = \sum_{l=0}^{L}\sum_{r=-l}^{l} R_{\alpha}\left(\varphi_a,\mu_p\right)\bar{q}_i^{g,\alpha}. \tag{26}$$

Substituting Eq. (26) into (23) yields the following two constraints

$$\sum_m \omega_m R_{\alpha}\left(\varphi_a,\mu_p\right)R_{\alpha'}\left(\varphi_a,\mu_p\right) = \delta_{\alpha\alpha'} \tag{27}$$

and

$$\delta A_a\sum_k t_{a,k,i} = V_i. \tag{28}$$

The first constraint, given by Eq. (27), requires the orthogonality of the real spherical harmonics function as a constraint on the angular quadrature used in the MOC calculation. This first constraint has already been discussed in detail by other authors [10]. The second constraint, given by Eq. (28), places a constraint on the renormalization of the tracks such that the region volume is conserved. In other words, the directional-dependent renormalization is a necessary, though not sufficient, requirement for particle conservation. In practice, typical MOC calculations by default use a very fine angular discretization, which result in

these constraints being satisfied to within a small criterion, e.g., $\left| V_i - \delta A_a \sum_k t_{a,k,i} \right| < \varepsilon$.

7. Particle Conservation and the Linear Source MOC

A generalization of the constraint given by Eq. (23) is introduced for the case of the LS MOC. Instead of considering the anisotropic source case from the start, the isotropic case will first be examined. The constraint requires the track-based linear sources to integrate exactly to the region-averaged isotropic source,

$$\left\langle 1, q^g_{m,k,i}\left(s_m\right)\right\rangle_i = \bar{q}^g_i \tag{29}$$

where $q^g_{m,k,i}\left(s_m\right)$ is given by Eq. (2). Setting $s_m \to t_m$ and $s_{m,k,i} \to t_{m,k,i}$ in Eq. (2) and substituting into Eq. (29), along with Eq. (11), yields the following constraints

$$\sum_a \omega_a \delta A_a \sum_k t_{a,k,i} = V_i \tag{30a}$$

$$\sum_a \omega_a \delta A_a \sum_k x^c_{a,k,i} t_{a,k,i} = 0 \tag{30b}$$

$$\sum_a \omega_a \delta A_a \sum_k y^c_{a,k,i} t_{a,k,i} = 0 . \tag{30c}$$

Since the LS MOC is based on the idea that high-order spatial moments of the source may be obtained by imposing a generalization of the particle balance, analogous constraints to that given by Eq. (29) are introduced in which the track-based linear source should exactly integrate to the region-wise spatial moments, which are given by Eq. (14)

$$\left\langle x, q^g_{m,k,i}\left(s_m\right)\right\rangle_i = Q^g_{i,x} \tag{31a}$$

$$\left\langle y, q^g_{m,k,i}\left(s_m\right)\right\rangle_i = Q^g_{i,y} . \tag{31b}$$

Setting $s_m \to t_m$ and $s_{m,k,i} \to t_{m,k,i}$ in Eq. (2) and substituting into Eqs. (31), along with Eq. (11), yields the following constraints

$$q^g_{i,x} M_{i,xx} + q^g_{i,y} M_{i,xy} = Q^g_{i,x} \tag{32a}$$

$$q^g_{i,x} M_{i,xy} + q^g_{i,y} M_{i,yy} = Q^g_{i,y} \tag{32b}$$

where coefficients $M_{i,xx}$, $M_{i,yy}$, and $M_{i,xy}$ [6] have already been introduced in the context of the LS MOC.

The entire LS MOC scheme is predicated on the set of constraints specified by Eqs. (30) and (32). In particular, directional-dependent (or independent) track renormalization results in satisfying the constraint given by Eq. (30a). The computation of the directional-dependent centroids given by Eqs. (8) automatically satisfies Eq. (30b) and (30c). Alternatively, direction-independent centroids, defined as X^c_i and Y^c_i [6], will also satisfy the constraints given by Eqs. (30b) and (30c). Finally, the constraints given by Eqs. (32) are identical to the 2×2 linear system of equations used to solve for the expansion coefficients in Eq. (11) [6, see Eq. (22)].

In summary, *the isotropic-source LS MOC scheme with direction-independent track renormalization and centroids satisfies the zeroth- and first-order particle balance equations, and therefore respects particle balance.*

Now consider the case of an anisotropic source. The constraint requires the track-based linear sources to integrate exactly to the region-averaged angular moment of the anisotropic source,

$$\left\langle 1, R_\alpha\left(\varphi_a, \mu_p\right) q^g_{m,k,i}\left(s_m\right)\right\rangle_i = \bar{q}^{g,\alpha}_i \tag{33}$$

where $q^g_{m,k,i}\left(s_m\right)$ is given by Eq. (2). Setting $s_m \to t_m$ and $s_{m,k,i} \to t_{m,k,i}$ in Eq. (2) and substituting into Eq. (33), along with Eq. (18), yields the following constraints

$$\delta A_a \sum_k t_{a,k,i} = V_i \tag{34a}$$

$$\delta A_a \sum_k x^c_{a,k,i} t_{a,k,i} = 0 \tag{34b}$$

$$\delta A_a \sum_k y^c_{a,k,i} t_{a,k,i} = 0 \tag{34c}$$

where the angular moments of the region-averaged anisotropic source are defined as follows

$$\sum_m \omega_m R_\alpha\left(\varphi_a, \mu_p\right) \bar{q}^g_{i,m} = \bar{q}^{g,\alpha}_i . \tag{35}$$

Analogous constraints to Eq. (33) exist in which the track-based linear source should exactly integrate to the spatial moments of each angular moment of the anisotropic source. However, since the LS MOC for anisotropic sources only considers the zeroth-order angular moment (or scalar) flux as possessing spatially-linear expansion coefficients, Eqs. (32) are again evaluated and the resulting constraint is identical to the 2×2 linear system of equations used to solve for the expansion coefficients in Eq. (18). Unlike the cases involving isotropic sources, the anisotropic case requires direction-dependent track renormalization and centroids, as seen from Eqs. (34). In practice, the MOC calculations by default use a very fine angular discretization, which result in these constraints being satisfied to within a small criterion, e.g., $\left| V_i - \delta A_a \sum_k t_{a,k,i} \right| < \varepsilon$, just as in the case of anisotropic scattering and the FS MOC.

In summary, *the anisotropic-source LS MOC scheme with direction-dependent track renormalization and centroids satisfies the zeroth- and first-order particle balance equations, along with the angular moments of the source, and therefore respects particle balance.* The use of direction-dependent track renormalization and centroids are necessary, though not sufficient, conditions for particle conservation.

Before leaving this section it is worthwhile to note that particle conservation could still be achieved, but at the cost of losing the orthogonality property of the spherical harmonic

function for anisotropic sources. This may result in requiring the inversion of a local matrix, which may be ill-conditioned [11], in order to obtain expansion coefficients from the angular moments.

III. NUMERICAL TESTS

The LS MOC scheme presented above possesses several properties which result in particle conservation. In this section a numerical verification of the properties is first performed by considering a simple pin cell problem. Following the verification, a set of realistic test problems are considered in order to evaluate the relative merits of the direction-dependent and independent normalizations for the FS and LS MOC. A test version of the CASMO5 lattice physics code is used in this section [2].

1. Pin Cell Verification Exercise

Consider a 4% U-235 enriched UO_2 pin cell problem consisting of a fuel pin with a 0.41 cm radius surrounded by moderator in a 1.26 cm pin pitch at room temperature. A spatial mesh consisting of 12 source regions is overlaid on the pin cell geometry. A set of angular directions consisting of 8 azimuthal angles and 1 polar direction is used to solve the problem. The final azimuthal angles and spacing are internally resolved by the code given a coarse ray spacing guess of 0.5 cm which will respect reflective boundary conditions. A schematic of the resulting tracking layout is depicted in Figure 1 below.

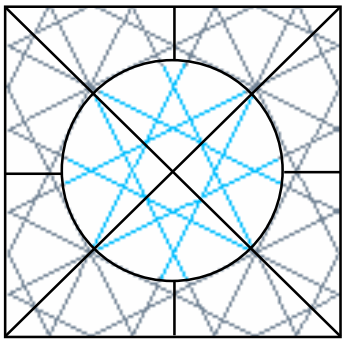

Fig. 1. Two-region pin cell problem using coarse angular quadrature.

In order to further simplify the problem and maintain some of the basic physics, group condensation is set to collapse the multi-group cross sections from the library group structure into an eight energy-group set. A total of four MOC options for solving the 2D transport equation are used in this exercise: isotropic source FS, isotropic source LS, anisotropic source FS, and anisotropic source LS. For simplicity, a Power Iteration (PI) scheme is used for the solution of the eigenvalue problem. The relative convergence criteria of the group-wise region-averaged scalar flux is set to $< 10^{-5}$.

The selection of a coarse angular quadrature is based on the observation that using few directions and coarse ray spacing should satisfy the constraints given by Eqs. (23), (24), (29), and (33) provided that track renormalization (and centroids) are computed consistently.

The results for the isotropic-source case are summarized in Table I. The first column refers to the MOC source representation (either FS or LS) and the second column refers to the renormalization of the tracks and centroids as either direction-independent (ISO) or by direction (AZI). All four cases converge in the same of number outer iterations, and the *maximum* absolute and relative differences between the region-averaged isotropic source and the integrated track source, following Eqs. (24) and (29), are below single precision. As described above, the necessary conditions for particle conservation in the case of an isotropic source given by Eqs. (30) are equally satisfied by either track renormalization and centroid options (ISO or AZI).

Table I. Numerical results of pin cell problem for isotropic sources.

MOC	Norm	Itrs.	Abs. diff.	Rel. diff.
FS	ISO	21	5.8E-09	3.2E-08
	AZI	21	4.0E-09	1.1E-08
LS	ISO	21	5.8E-09	3.3E-08
	AZI	21	4.8E-09	1.7E-08

In the case of anisotropic sources, an additional constraint is required for particle conservation, which involves the orthogonality of the spherical harmonics function, given by Eq. (27). This condition was numerically verified by considering an anisotropic source case in which $L=1$ for the anisotropic scattering order. It is trivial to verify that the evaluation of the spherical harmonics orthogonality property is satisfied for the set of angles used in this exercise. In a similar fashion to the isotropic source, the anisotropic source results are tabulated in Table II. All four cases converge in the same number of outer iterations, and the absolute and relative differences between the region-averaged anisotropic source and the integrated track source angular moments, following Eqs. (23) and (33), were calculated. In this instance, the table lists the *maximum* absolute and relative differences, not only over all groups and regions, but also over all three angular moments of the source.

Table II. Numerical results of pin cell problem for anisotropic sources and $L=1$.

MOC	Norm	Itrs.	Abs. diff.	Rel. diff.
FS	ISO	25	8.9E-04	7.3E-02
	AZI	25	1.2E-07	2.1E-05
LS	ISO	25	9.2E-04	7.3E-02
	AZI	25	1.3E-07	8.8E-05

The numerical results shown in Table II indicate that errors (up to 7%) may be encountered in the evaluation of the angular moments of the source if direction-independent renormalization is used for problems involving anisotropic sources.

Refining the ray spacing results in an improved estimation of the angular moments of the source for the direction-independent renormalization. In an analogous fashion, refining the number of angles in the azimuthal plane further reduces the differences, thereby preserving all three source angular moments to within single precision in the limit of many directions. A summary of the numerical results from such an angular refinement study is shown below in Table III. As the number of azimuthal angles is increased, the ray spacing must also be decreased in order to obtain rays crossing the boundary of the problem for 'small' angular directions.

Table III. Numerical results of pin cell problem for anisotropic sources and $L=1$ with angular refinement.

MOC	Norm	Itrs.	a	δA_a	Abs. diff.	Rel. diff.
FS	ISO	24	16	0.25	1.4E-04	1.6E-02
		23	32	0.1	1.0E-04	8.1E-03
		23	64	0.05	2.7E-05	2.3E-03
		23	128	0.01	3.9E-06	1.8E-04
FS	AZI	24	16	0.25	1.4E-07	6.3E-05
		23	32	0.1	1.5E-07	6.9E-05
		23	64	0.05	1.7E-07	4.0E-05
		23	128	0.01	1.9E-07	3.8E-05
LS	ISO	24	16	0.25	1.6E-04	1.6E-02
		24	32	0.1	1.3E-04	8.1E-03
		24	64	0.05	3.3E-05	1.9E-03
		24	128	0.01	3.9E-06	1.6E-04
LS	AZI	24	16	0.25	1.1E-07	9.8E-05
		24	32	0.1	1.4E-07	2.2E-05
		24	64	0.05	1.4E-07	1.1E-04
		24	128	0.01	1.2E-07	4.0E-05

Finally, setting the anisotropy order to $L=5$, refining the angular quadrature to 128 azimuthal angles and 5 polar angles (Gauss-Legendre quadrature), and setting a target 0.01 cm ray spacing allows for the comparison of the several options over the entire set of twenty-one angular moments. The refined angular quadrature is necessary in order to satisfy the orthogonality property of the spherical harmonics in the numerical evaluation. A summary of the results is shown in Table IV below.

Table IV. Numerical results of pin cell problem for anisotropic sources and $L=5$.

MOC	Norm	Itrs.	Abs. diff.	Rel. diff.
FS	ISO	24	4.8E-04	1.4E+01
	AZI	24	2.3E-07	2.5E-03
LS	ISO	24	4.7E-04	1.6E+01
	AZI	24	2.1E-07	2.7E-03

The absolute differences for the ISO cases indicate an acceptable level of precision, although clearly the AZI option achieves consistency to within single precision. The large relative differences in the ISO cases correspond to higher angular moments, which are rather small in terms of their absolute value. Therefore, they are expected to have little impact on the accuracy of the numerical solution.

2. Evaluation of B&W-1484 Core I & II

Particle conservation can be achieved by direction-independent renormalization of the tracks (and centroids calculation) for both FS and LS MOC when considering isotropic source. In the case of anisotropic sources, directional quantities must be computed in order to satisfy the constraint regardless of the angular quadrature being used. Storage requirements for renormalization factors (and centroid) increase by the number of azimuthal directions for the FS and LS MOC. This might become significant for the LS MOC since it involves three direction-dependent quantities times the number of source region. Therefore, an evaluation of the additional storage requirements is necessary for realistic applications. The results shown in this section are limited to two-dimensional geometry, but may provide some indication of what might be encountered for a three-dimensional LS MOC implementation.

Following previous analysis of the B&W-1484 [6], updated models accounting for the detailed non-symmetric geometry, compositions and conditions are considered in the evaluation of the LS MOC schemes.

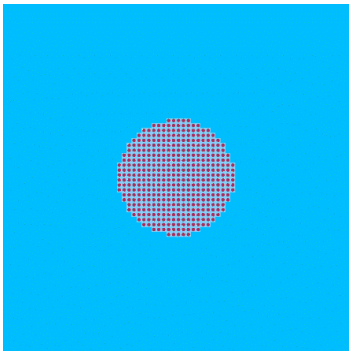

Fig. 2. B&W-1484 Core I geometry.

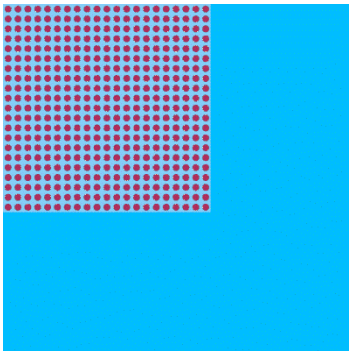

Fig. 3. B&W-1484 Core II geometry.

The Core I & II geometry is depicted in Fig. 2 & 3. Core I consists of 458 fuel pins arranged in a circular shape and is designed to be in a very high-leakage configuration. Core II consists of 1764 identical fuel pins arranged in a square shape and is designed to be in a relatively low-leakage configuration.

The transport calculations performed for the Core I & II used a 95 energy-group structure and an effective axial buckling, which is used to capture the effects of leakage in three dimensions. The anisotropic source treatment relied on the expansion of the scattering source up to $L = 3$, which resulted in the computation of a total of ten angular moments of the flux. The angular discretization is based on the default 64 azimuthal angles and 0.05 cm ray spacing. A summary of the results is presented in Table V and the fission distributions are depicted in Figs. 4 & 5.

Table V. Results for B&W-1484 Core I & II with anisotropic sources.

Core	Norm	K-effective	Rel. Mem.	Rel. Time
I	ISO	0.99921	1.0	1.0
	AZI	0.99921	1.01	0.991
II	ISO	1.00086	1.00	1.0
	AZI	1.00086	1.01	0.992

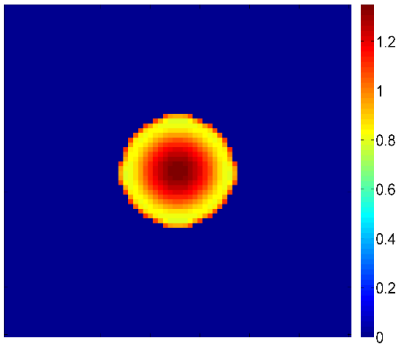

Fig. 4. B&W-1484 Core I normalized fission distribution.

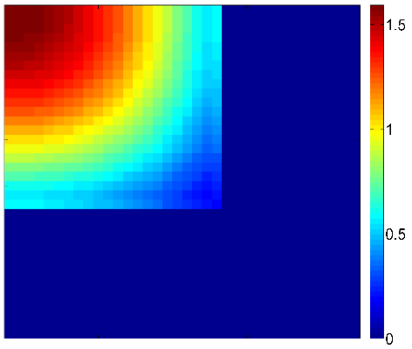

Fig. 5. B&W-1484 Core II normalized fission distribution.

The resulting eigenvalue (K-effective) indicates that for realistic numerical transport calculations there is practically no difference between the renormalization and centroid definitions when considering anisotropic sources. Although not shown in this section for brevity, it is worthwhile to note that both options (ISO and AZI) converged in exactly the same number of transport sweeps and the final fission distribution was identical. The relative memory requirements and run time, tabulated in Table V, indicate that performing direction-dependent renormalization (and centroid calculation) results in a slight decrease in the run time accompanied by an increase in memory (storage) requirements. Therefore, the use of such direction-dependent definitions may not constitute an exorbitant increase in resources.

The fission distributions were compared to those resulting from a transport-corrected P0 (TRN) and an uncorrected P0 calculations (NONE.) The results are tabulated in Table VI and indicate that good agreement may be achieved by using the transport-corrected P0 approximation, whereas neglecting any correction clearly results in unacceptable results.

Table VI. Results for B&W-1484 Core I & II with isotropic sources. (Relative to $L = 3$ results.)

Core	P0	K-effective	Delta-k	Max. % Diff.
I	NONE	1.04102	4181	11.5
	TRN	1.00076	155	1.7
II	NONE	1.10176	10090	25.0
	TRN	1.00082	-4	0.6

The transport-corrected P0 approximation used in CASMO5, which is based on the inflow formulation and used for several decades, is discussed in detail in various other publications, including [12].

3. Evaluation of Quarter-Core 17x17 PWR

In order to verify memory and run-time penalties incurred by using the direction-dependent schemes (relative to the direction-independent option) a quarter-core geometry of a hypothetical PWR core constituted of typical 17x17 fuel assemblies was modeled using CASMO5. The default angular quadrature was used in the calculation in conjunction with a detailed 95 energy-group structure and a $L = 3$ anisotropic source expansion order. The quarter-core geometry generated from the ray-tracing is depicted in Fig. 6, which includes the explicit modeling of the baffle, core barrel and pad.

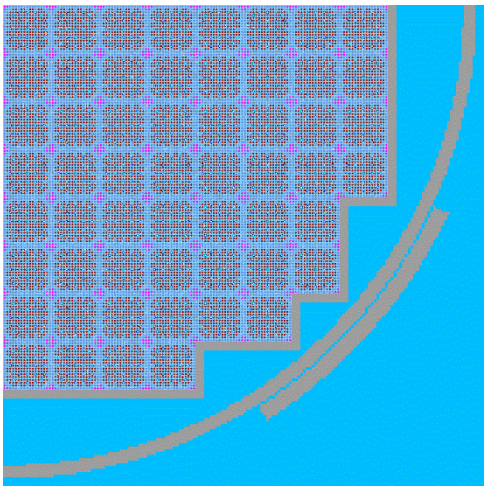

Fig. 6. Two-dimensional PWR core geometry.

Some degree of multi-processing is necessary when performing large calculations in order to reduce the wall-clock time to a reasonable level. Using the multi-threading OpenMP capabilities implemented into CASMO5 [2], which relies on the angular decomposition of the MOC transport sweep, a total of 8 cores were utilized in the calculation which resulted in a speed-up proportional to a factor of 7. The resulting fission distribution is depicted in Fig. 7. It is worthwhile to note that fresh assemblies involving identical enrichment were used in this hypothetical core, therefore the resulting fission distribution (proportional to power) is not flat as expected in realistic core designs.

The resulting eigenvalues, corresponding to the ISO and AZI options, were found to be within ~1 pcm difference, which is considered to be in good agreement given the size of the problem. The total number of transport sweeps performed was found to be identical between the two cases. A comparison of the memory requirements during execution indicates an increase in the relative memory resource usage of approximately 1.4% when using the AZI option relative to the ISO option. This estimate was verified by comparing an internal tally of maximum memory usage the code provides in the output. Finally, the relative wall-clock time used by the calculation using the AZI option, relative to the ISO option, is approximately 0.93. In other words, the use of the AZI option shows a reduction in terms run-time of approximately 7% relative to the ISO option.

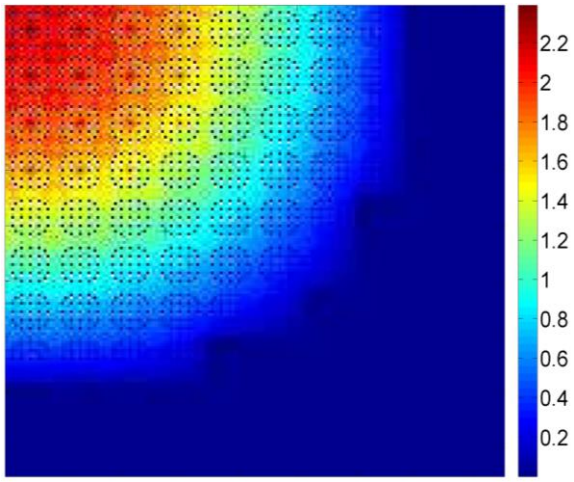

Fig. 7. Two-dimensional PWR core fission distribution.

IV. CONCLUSIONS

The developments summarized in this work indicate that direction-independent track renormalization and centroid definitions result in particle conservation when applying the LS MOC scheme to problems involving isotropic sources. In the case of anisotropic sources, direction-dependent renormalization and centroids are required to respect conservation. Various examples are presented which numerically verify the theory behind particle conservation for LS MOC. In addition, realistic two-dimensional transport problems involving anisotropic scattering and many energy groups are used to evaluate the impact of using direction-dependent track renormalization and centroids. The results indicate practically no difference in terms of convergence, eigenvalue or fission distributions between the two

approaches. This is due to the very fine angular quadrature used in CASMO5 by default, which diminishes the inconsistencies, as shown in the numerical results. However, a slight increase in relative memory requirements is observed due to the direction dependence of the renormalization and centroids, relative to the direction-independent case. The slight increase in memory requirements is accompanied by a reduction in the total wall-clock time due to the cancellation of various quantities when considering direction-dependent centroids.

Given the emphasis on particle conservation from a theoretical perspective, the results presented here indicate that is not prohibitive to consider direction-dependent renormalization and centroids in a practical LS MOC implementation involving anisotropic scattering. Implementations involving three-dimensional FS/LS MOC and anisotropic sources should consider an analogous evaluation of the track renormalization (and centroids) if such an approach is under consideration.

NOMENCLATURE

MOC = Method of Characteristics
FS = Flat Source
LS = Linear Source
ISO = isotropic or direction-independent normalization
AZI = azimuthal or direction-dependent normalization

REFERENCES

1. D. KNOTT, "KRAM, A Lattice Physics Code for Modeling the Detailed Depletion of Gadolinia Isotopes from BWR Fuel Designs," Ph.D. Thesis, The Pennsylvania State University (1991).
2. R. FERRER, J. HYKES, and J. RHODES, "CASMO5, A Fuel Assembly Burnup Program: Methodology Manual," SSP-08/405 Rev. 6, Studsvik Scandpower, Inc. (2017).
3. B. KOCHUNAS, "A Hydrid Parallel Algorithm for the 3-D Method of Characteristics Solution of the Boltzmann Transport Equation on High Performance Computing Clusters," Ph.D. Thesis, University of Michigan, (2013).
4. S. SHANER, G. GUNOW, B. FORGET, and K. SMITH, "Verification of the 3D Method of Characteristics Solver in OpenMOC," *Proc. PHYSOR 2016*, Sun Valley, Idaho, May 1–5, 2016, American Nuclear Society (2016) (CD-ROM).
5. G. GUNOW, J. TRAMM, B. FORGET, K. SMITH, and T. HE, "SimpleMOC – A Performance Abstraction for 3D MOC," *Proc. M&C 2017*, Nashville, Tennessee, April 19–23, 2015, American Nuclear Society (2015) (CD-ROM).
6. R. FERRER and J. RHODES, "A Linear Source Approximation Scheme for the Method of Characteristics," *Nucl. Sci. Eng.*, **182**, 151 (2016).
7. K. SMITH and J. RHODES, "Full-Core, 2D, LWR, Core Calculations with CASMO-4E," *Proc. PHYSOR 2002*, Seoul, Korea, October 7–10, 2002, American Nuclear Society (2002) (CD-ROM).
8. R. FERRER, J. RHODES, and K. SMITH, "Linear Source Approximation in CASMO5," *Proc. PHYSOR 2012*, Knoxville, Tennessee, April 15–20, 2012, American Nuclear Society (2012) (CD-ROM).
9. R. FERRER and J. RHODES, "Extension of the Linear Source MOC Methodology to Anisotropic Scattering in CASMO5," *Proc. PHYSOR 2014*, Kyoto, Japan, September 28–October 3, 2014, American Nuclear Society (2014) (CD-ROM).
10. R. LE TELLIER and A. HÉBERT, "Anisotropy and Particle Conservation for Trajectory-Based Deterministic Methods," *Nucl. Sci. Eng.*, **158**, 28 (2008).
11. A. HÉBERT, "High-Order Diamond Differencing Along Finite Characteristics," *Nucl. Sci. Eng.*, **169**, 81 (2011).
12. Z. LIU, K. SMITH and B. FORGET, "A Cumulative Migration Method for Computing Rigorous Transport Cross Sections and Diffusion Coefficients for LWR Lattices with Monte Carlo," *Proc. PHYSOR 2016*, Sun Valley, Idaho, May 1–5, 2016, American Nuclear Society (2016) (CD-ROM).